Pergamon

PII: S0038-092X(96)00083-7

Solar Energy Vol. 58, No. 4–6, pp. 227–237, 1996

0038-092X/96 $15.00 + 0.00

FLOW DISTRIBUTION IN UNGLAZED TRANSPIRED PLATE SOLAR AIR HEATERS OF LARGE AREA

L. H. GUNNEWIEK,† E. BRUNDRETT and K. G. T. HOLLANDS
Department of Mechanical Engineering, University of Waterloo, Waterloo, Ontario, Canada N2L 3G1,

(Communicated by Doug Hittle)

Abstract—Unglazed transpired plate solar air heaters have proven to be effective in heating outside air on a once-through basis for ventilation and drying applications. Outside air is sucked through unglazed plates having uniformly distributed perforations. The air is drawn into a plenum behind the plate and then supplied to the application by fans. Large collectors have been built that cover the sides of sizeable buildings, and the problem of designing the system so that the air is sucked uniformly everywhere (or nearly so) has proven to be a challenging one. This article describes an analytical tool that has been developed to predict the flow distribution over the collector. It is based on modelling the flow-field in the plenum by means of a commercial CFD (computational fluid mechanics) code, incorporating a special set of boundary conditions to model the plate and the ambient air. This article presents the 2D version of the code, and applies it to the problem of predicting the flow distribution in still air (no wind) conditions, a situation well treated by a 2D code. Results are presented for a wide range of conditions, and design implications are discussed. An interesting finding of the study is that the heat transfer at the back of the plate can play an important role, and because of this heat transfer, the efficiency of a collector in non-uniform flow can can actually be greater than that of the same collector in uniform flow. Copyright © 1996 Elsevier Science Ltd.

1. INTRODUCTION

Daytime heating of fresh air for industrial work spaces and for crop drying are two important applications where a non-storage solar system can be beneficially used to heat ambient air directly on a once-through basis. Since the late 1980s a promising solar air heating system has been developed and commercialized for just this type of application (Fig. 1). The system's collector—called an unglazed transpired plate, or UTP, collector—consists of a perforated plate built onto a southward facing wall. Using traditional building methods, the plates are fastened to the wall with standoff hardware, thereby leaving a plenum behind the plates. The plenum is connected to a fan which provides suction pressure and also positive pressure to deliver the heated air to the load, e.g. to the factory floor, via a manifold system. Tests conducted on a prototype installation indicated that such an unglazed collector would be practical (Carpenter and Kokko, 1991). Since then, large scale systems totalling thousands of square metres have been installed and successfully operated for fresh-air heating in Canada, the United States, and Germany (Hollick, 1994).

The essence of the design is the use of construction-grade technologies to produce a low cost, robust solar heating system. However, the collector is also based on sound heat transfer principles (Kutscher *et al.*, 1993). It is efficient because the convective heat loss to the air in front of the plates is later recaptured when the boundary layer is sucked into the plenum, and

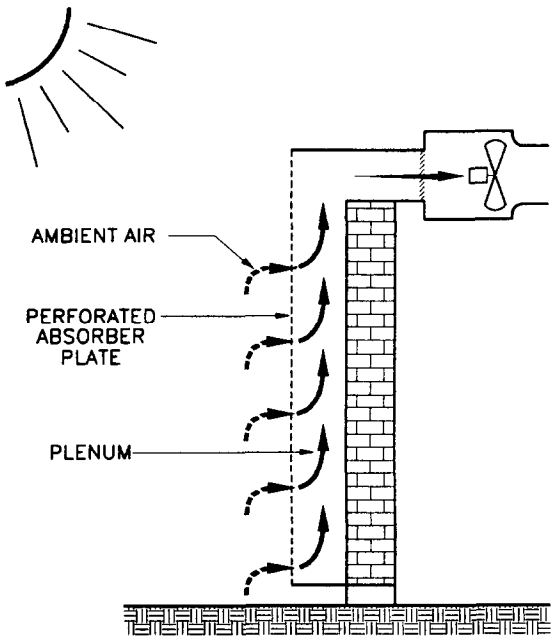

Fig. 1. Drawing of unglazed transpired plate (UTP) collector installed on a vertical wall.

†Presently at Hatch Associates Ltd., 2800 Speakman Drive, Sheridan Science and Technology Park, Mississauga, Ontario, L5K 2R7, Canada.

the intimate heat transfer to this boundary layer keeps the plate temperature low, thereby reducing radiant heat loss to an acceptable level.

While models for the local heat transfer at the plate have been developed in some detail (Kutscher, 1994; Cao *et al.*, 1993; Golneshan, 1995), modelling the overall performance has received less attention. The main item determining this overall performance is the uniformity of the flow across the whole collector face. It is known that poor distribution can cause local hot spots, where the radiative losses will dominate (Kokko and Marshal, 1992). Indeed, on some parts of the collector, the flow may actually be out of the plate, instead of in (this is called flow reversal), meaning that not only is the solar energy absorbed on that part of the plate totally lost, but some of the energy already collected in other parts of the plate is also lost. Dymond and Kutscher (1995) recently analyzed flow distribution using a "pipe network" model. While capable of fast simulation on a PC, such a model is of uncertain accuracy, as it replaces the actual plenum by a system of short lengths of pipes. More accurate would be a model that solves the fundamental equations of conservation of mass, momentum, and energy, through a computational fluid dynamics (CFD) code. While unrealistically slow for design work, such an approach would provide fundamental insights and a valuable research tool that could be used, for example, for calibrating the pipe network model.

The present article describes the first step in the development of a suitable CFD model. The complete model is a 3D one, capable of modelling the whole plenum flow, including the effects of the wind (Gunnewiek, 1994). We present in this article a description of only the 2D version, which can account for variations in the plenum flow only in the vertical direction. This version is ideal for studying the effect of buoyancy, which is a major cause of flow maldistribution.

2. DEVELOPMENT OF THE CFD MODEL

2.1. Overview

The basic CFD code (TASCflow Version 2.2) used was provided by Advanced Scientific Computing Ltd. TASCflow uses the finite volume procedure and follows in broad terms the methodology laid out by Patankar (1980) whereby the equations prescribing conservation of mass, momentum, and energy are discretized and solved in such as way as to be fully conservative of these quantities. A 3D code, it can be easily adapted to 2D problems, as in the present instance, and provides a full range of support features. The code provides for a number of platforms including the one used for this study, which was a Sun SPARC workstation computer with 48 Mb of memory.

Modelling a full-scale UTP collector mounted on a wall (Figs 1 and 2) required some simplifications in order to fit the model grid within the limits of the computer. The approach used was to include only the plenum region (i.e. the H by D by W region in Fig. 2) in the computational domain of the code, and to model the plate and the ambient surrounds by means of a pair of special boundary conditions applied at the domain's front-face, i.e. at the boundary at $x = t$. The first of these front-face boundary conditions was essentially an energy balance on the plate that included the absorbed solar radiation, the radiation to the surrounds, and a model for the plate-to-air heat transfer rate. The second was essentially a momentum balance that incorporated a model for the hydraulic resistance of the plate and for the pressure distribution at the exterior face of the plate. The two boundary conditions were not standard TASCflow boundary conditions, but were specially coded for the present task by Advanced Scientific Computing Ltd.

The transpiration of air through the plate was modelled as a continuous phenomena rather than as a process occurring through discrete holes. Without this simplification the problem would not have been solvable in any reasonable time—the work of Cao *et al.* (1993) having shown that modelling the flow around

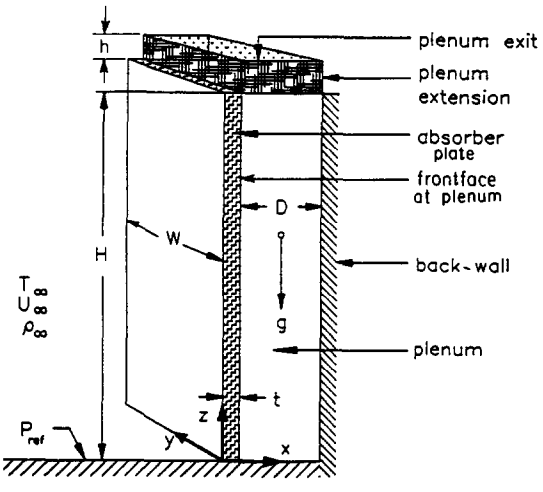

Fig. 2. Dimensioned sketch of the UTP's plenum.

even a single hole required several hours of computer time and a highly refined grid. The same study showed that the velocity profiles are smooth within a short distance of the holes so the errors associated with this simplifying assumption should be modest.

2.2. *Front-face boundary-conditions*

Momentum balance. Literature models for the local pressure drop across a perforated plate, ΔP_p, as a function of the approach velocity, u_s, were examined in detail (Gunnewiek, 1994). To make the results of the present study applicable to the largest range of plate porosities, plate thicknesses, and hole shapes and diameters possible, it was decided to model only the parametric form of this function, the values of the actual parameters being evaluated later for the particular plate at hand. A suitable form was found to be

$$\Delta P_p = \rho K_H u_s^n \tag{1}$$

where n and K_H are the parameters. This model captures the well-known equations for ΔP_p that apply in the limiting cases of very high hole Reynolds number (where $n=2$) and very low hole Reynolds number (where $n=1$). Fitting eqn (1) to the long-orifice plate correlation function of Licharowicz *et al.* (1965), assuming typical values of porosity, thickness, and hole diameter, gave a value of $n=1.5$ over a wide range of velocities of interest, so at least for the purpose of the present study, this value of n of 1.5 was used. For $n=1.5$, the values of K_H (called the plate's hydraulic impedance) were found to range between 750 and 3750 $(m/s)^{1/2}$. (In practice, one can find K_H for a particular plate by evaluating ΔP_p from some suitable equation, such as that of Licharowicz *et al.* (1965) or Kutscher (1994), using u_{ave} for u_s, and then solving eqn (1) for K_H.)

The front-face pressure was obtained from the ambient hydrostatic pressure as follows:

$$P(0,z) = P_{ref} - \rho g z \tag{2}$$

where the first term on the right hand side is the ambient pressure at ground level. It is now assumed that eqn (1) applies locally, so u_s is now the local face velocity at $x=t$: i.e. $u_s = u(t,z)$, called the suction velocity, and also ΔP_p is the local pressure difference $P(0,z) - P(t,z)$, where $P(0,z)$ is given by eqn (2). Thus combining eqns (1) and (2) one obtains a relation between the x-velocity and the pressure at $x=t$, which is the momentum balance front-face boundary-condition. The non-slip boundary condition $v(t,z)=0$ is also assumed to apply at the front-face.

Energy balance. The plate boundary layer is assumed to be in the asymptotic region (Kutscher, 1991) over the whole collector, so long-wave radiation is assumed to be the only heat loss. An energy balance† on the plate gives

$$\alpha G = \rho C_p u(t,z)(T(t,z) - T_\infty) + h_r(T_p(z) - T_\infty) + (q_b/A) \tag{3}$$

where q_b is the heat flow (assumed uniform) at the back of the plate, which can occur by convection to the air in the plenum. The plate temperature $T_p(z)$ can be expressed in terms of the plate heat exchange effectiveness ϵ_{HX} (Kutscher, 1994; Cao, 1993), which is defined by

$$\epsilon_{HX} = (T(t,z) - T_\infty)/(T_p(z) - T_\infty) \tag{4}$$

and which is a measure of the intimacy of heat transfer between the air and the plate. Combining eqns (3) and (4) gives the energy-balance front-face boundary-condition:

$$T(t,z) = T_\infty + (\alpha G)_n/(\rho C_p u(t,z) + U_o) \tag{5}$$

where U_o is h_r/ϵ_{HX}, and $(\alpha G)_n$ is the net of the absorbed solar radiation and the back-of-the-plate heat transfer: $(\alpha G)_n = \alpha G - q_b/A$. Both h_r and ϵ_{HX} are relatively insensitive to suction velocity (as well to other system variables, such as solar radiation, ambient temperature, etc.), so we will treat U_o as a constant for a given simulation, and as a parameter of the total study. Also, the q_b could not be established a priori, so it was determined a posteriori, as will be explained later. We consider $(\alpha G)_n$ to be one of the parameters of the problem.

(It should be noted that there is a slight inconsistency in the derivation of this energy-balance boundary-condition, in that the plate temperature has been made different from the temperature of the air emerging from the holes. This approach will be strictly true only in the limit of ϵ_{HX} = unity, i.e. for continuous suction.)

2.3. *Further aspects of the plenum model*

The fan downstream of the plenum was assumed to produce a prescribed total flow Q m^3/s, to have a uniform velocity profile at its inlet, and to be connected to the plenum by

†Equation (3) assumes the surrounds temperature T_s is equal to ambient air temperature T_∞. If this is not the case, $h_r(T_s - T_\infty)$ should be added to (αG).

means of a straight, slip-wall, adiabatic extension of height h, as shown by hatched lines in Fig. 2. The computational domain was extended to include this extension. It was found that for $h > 0.11H$, the flow in the plenum was independent of the actual value of h chosen, and all subsequent simulations were made to satisfy this condition on h. Indeed, none of these assumptions about the nature of the items downstream of the plenum would be expected to significantly effect the plate flow uniformity, which was the quantity of interest.

In addition to the boundary conditions described so far, others must be prescribed: The plane $x = D + t$ represents the wall on which the collector is mounted, and this is expected to be well-insulated, so this face was modelled as adiabatic and, of course, as non-slip. The same is true of the floor plane, $z = 0$. This completes the boundary-condition specification.

TASCflow requires the user to specify either laminar or turbulent flow, and if turbulent, a turbulence model must be chosen. The plenum Reynolds number based upon the hydraulic diameter and average velocity varied from zero at the bottom of the plenum to a maximum at the top. An examination of expected Reynolds numbers indicated that the majority of the plenum flow would be turbulent for all cases, based upon classical smooth pipe observations. Further, the jetting action at the suction holes in the plate would probably induce early transition. Thus a turbulence model was indicated, and the TASCflow $k-\epsilon$ model was chosen.†

2.4. *Parametric range studied*

A suitable range of parameters to be studied was determined by examining the current technology and possible future extensions to it. The collector height range was $3.0 \leq H \leq 6.0$ m, and the plenum aspect ratio range was $10 \leq H/D \leq 50$. The range of U_o was $1.0 \leq U_o \leq 9.0$ W/m^{2}K. (This represents the range from a non-selective surface plate with low heat exchanger effectiveness with high losses for $U_o = 9.0$, to an absorber with a selective surface and a high heat exchange effectiveness for $U_o = 1.0$.) The range of Q (given in terms of the average suction velocity, $u_{ave} = Q/A$) was $0.005 \leq Q/A \leq 0.08$ m/s. The plate hydraulic impedance range was $750 \leq K_H \leq 3750$ (m/s)$^{0.5}$. Finally, the net absorbed solar irradiance range was $400 \leq (\alpha G)_n \leq 900$ W/m^2.

2.5. *Grid generation and refinement*

The first step in setting up the code is to generate the grid planes on which the nodal points (the points at the centres of the control volumes) are located. For convenience, the grid planes were made parallel to the three co-ordinate planes, so there were x-grid planes (parallel to the yz-plane), y-grid planes (parallel to the xz-plane) and z-grid planes (parallel to the xy-plane). The nodal points lie at the intersections of these three sets of planes. To make the 3D TASCflow code simulate the 2D problem, three y-grid planes were constructed: at $y = 0$, at $y = W/2$, and at $y = W$, and then symmetry boundary conditions are prescribed at the $y = 0$ and the $y = W$ planes.

Part of the art of placing the grid planes relates to the turbulence model. Turbulence modelling codes require all the nodal points to be in the fully turbulent region. For the points near the wall(s) this requires that they be in the logarithmic part of the wall boundary layer, a condition normally satisfied only if the distance d of the first node away from the wall is in the range $55\nu/k^{1/2} \leq d \leq 900\nu/k^{1/2}$, where k is the turbulent kinetic energy (solved for in the code) and ν is the kinematic viscosity. The largest d satisfying this condition (typically to be about $0.15D$) was found to occur at the bottom of the plenum, where k is smallest. Thus the distance from the plate to the first x-grid plane away from the plate and the distance from the back wall to the first x-grid plane away from the back wall were fixed on the basis of turbulence considerations, and grid generation then proceeded for the remainder.

It was determined that, for speedier convergence, the spacing between the remaining x-grid planes should not be constant but should increase with x. This was done in such a way that the ratio of adjacent spacings was held constant. This "expansion" is characterized through a TASCflow parameter R, which is the ratio that the spacing between the first and second x-grid planes out from the rear wall makes to the spacing between the first and second x-grid planes out from the plate. Keeping $5 \leq R \leq 10$ was found to concentrate sufficient flux elements near the front-face, where the flow is turning sharply, while reducing unnecessary

†It was pointed out during the review of this article that certain studies [e.g. Kays and Crawford (1980) and Kuroda and Nishioka (1989)] would indicate that the laminar assumption may have been a better one, because the flow in the plenum is accelerating. However, no previous study, to our knowledge, relates to this exact problem. More work is required to clarify this point.

computational labour near the back wall, without making the grid too coarse there. So, subsequent simulations kept R in this range. The z-grid planes were kept uniformly spaced.

The process of discretizing the governing equations introduces an error in the solution that decreases as the total number of nodal points N in the domain increases. A grid refinement study is normally carried out, in which a value of N large enough to ensure acceptable accuracy is determined. In the present study, we carried out the grid refinement study by comparing solutions obtained from three successively finer grids. The first grid, denoted $N1$, had 20 flux elements (or grid-plane spacings) in the x-direction, 3 flux elements in the y-direction (as required by TASCflow for 2D simulations) and 100 flux elements in the z-direction; we write this as $N1 = 20 \times 3 \times 100$. The remaining grids were $N2 = 30 \times 3 \times 150$, and $N3 = 40 \times 3 \times 200$. Extrapolation methods were then used to estimate the solution asymptote as $N \to \infty$, which is assumed to be the true solution, and the error of each of the three grids was thereby estimated. This grid refinement study was carried out for the following parametric settings: $H = 4.5$ m; $H/D = 30$; $Q/A = 0.02$ m/s; $K_H = 2250$ (m/s)$^{1/2}$, $(\alpha G)_n = 650$ W/m^2; and $U_o = 5$ W/m^2 K. The results showed that simulations obtained using the $N1$ grid should give answers for the local suction velocity that are within about 2% of the true value, for the mean gauge pressure at the collector top that are within 7% of the true value, and for the useful energy collected that are within 3% of the true value. Full details are given by Gunnewiek (1994). Since this accuracy was considered to be just commensurate with the current needs, and in view of the long simulation times required for the other grids, all subsequent 2D simulations reported in this article were carried out with the $N1$ grid.

3. RESULTS

The combined range of the six controlling parameters was covered by simulating certain combinations of the following values: $H = 3.0$, 4.5, 6.0 m; $(\alpha G)_n = 400$, 650, 900 W/m^2; $U_o = 1.0$, 5.0, 9.0 W/m^2 K; $Q/A = 0.005$, 0.01, 0.02, 0.04, 0.08 m/s; $H/D = 10$, 20, 30, 40, 50; and $K_H = 750$, 1500, 2250, 3000, 3750 (m/s)$^{1/2}$. Not all combinations were simulated. Rather a "typical configuration" was selected as one with the following "mid-line settings": $H = 4.5$ m, $(\alpha G)_n = 650$ W/m^2, $U_o = 5.0$ W/m^2 K, $u_{ave} = 0.02$ m/s, $H/D = 30$, $K_H = 2250$ (m/s)$^{0.5}$. Then each of the parameters was allowed to vary over its range, with the rest held constant at the mid-line values. Simulations were computed at each of the resulting combinations.

With a few exceptions, Figs 3 and 4 plot the simulated velocity profiles obtained for these various parametric settings. The quantity plotted is the normalized suction velocity, U^*, defined by $U^* = u(t,z)/u_{ave}$. The exceptions are those parametric combinations having $Q/A = 0.01$ and 0.005 m/s. All of the simulations having $Q/A = 0.005$ and most of those having $Q/A = 0.01$ were found to experience flow reversal near the top of the plate: that is, the flow there was out of the plate rather than into the plate. Reverse flow through any part of the plate is highly undesirable because none of the solar energy incident on this region is collected, and some of the energy that has already been collected over the rest of the plate is actually lost to the environment. Clearly flow reversal should be avoided in practice. That it can occur for these low values of Q/A is one of the more important findings of this study. The lowest Q/A that would not cause reverse flow over at least some of the range of the other parameters was found to be 0.0125 m/s, and so this setting was added to the list of settings simulated (see Fig. 4).

To physically interpret this reverse-flow result, as well as the profiles plotted in Figs 3 and 4, it is useful to think of the flow as the superposition of two flows: a buoyant flow driven by the temperature differences developed by the absorbed solar energy, and a forced flow developed by the fan. Acting on its own (i.e. with $Q = 0$) the buoyant flow would be in at the bottom of the collector and out at the top. In Figs 3 and 4, this flow is best illustrated by the profile shown in Fig. 4 for $Q/A = 0.0125$. In contrast, the forced flow acting on its own would produce a profile having less flow at the bottom and more at the top. In Figs 3 and 4 this flow is best illustrated by the profile shown in Fig. 4 for $Q/A = 0.08$. This shape of flow profile is well known in manifold design (Bajura and Jones, 1976) and is brought about by the plenum pressure's tendency to decrease in the vertical direction because the flow is accelerating in the plenum and because of friction along the plenum walls. Both acceleration and friction tend to increase as the plenum is made narrower, so the forced flow profile shape is also clearly

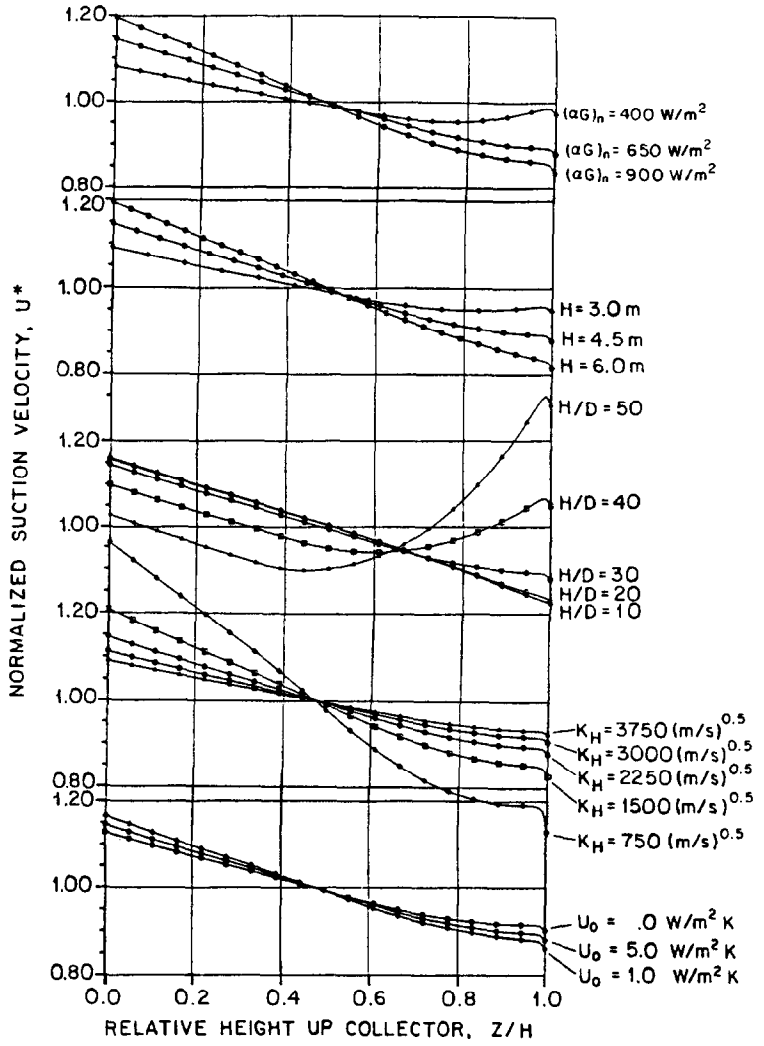

Fig. 3. Normalized suction velocity profiles for various parametric settings. Unless otherwise indicated, all parameters are at their mid-line values.

demonstrated at high H/D settings, e.g. by the $H/D=50$ profile in Fig. 3.

The fact that most of the flows illustrated in Figs 3 and 4 have more flow at the bottom and less at the top demonstrates that the buoyant flow is playing a very important role over most of the parametric range investigated. Buoyant effects would be expected to be most pronounced when the height H is greatest, and also when the net absorbed radiation $(\alpha G)_n$ is greatest, and this expectation is borne out in the Figures. The Figures also show that buoyancy effects tends to be reduced when Q/A is large (as would be expected). The buoyant effect is also seen to be reduced when the plate's hydraulic resistance K_H is large or when the aspect ratio H/D is large. This is because there is a limit to the equivalent pressure difference that buoyancy can develop (to overcome friction, either at the plenum walls or in the plate), whereas the forced flow, having fixed Q, is not restricted in this way, and hence it tends to dominate in these instances. The heat loss parameter U_o has only a very modest effect on the velocity profile; like the absorbed solar radiation, it has an effect (in this case somewhat modest) on the inlet temperature, and therefore on the buoyancy.

The profile of the temperature of the air entering the plenum, $T_i = T(t,z)$, is also of interest. When the velocity profile is completely uniform, this temperature, now denoted $T_{i,u}$, is also uniform, and is given by eqn (5) with $u(t,z)=u_{ave}$. We can form a normalized inlet temperature θ as

$$\theta=(T(t,z)-T_\infty)/(T_{i,u}-T_\infty) \qquad (6)$$

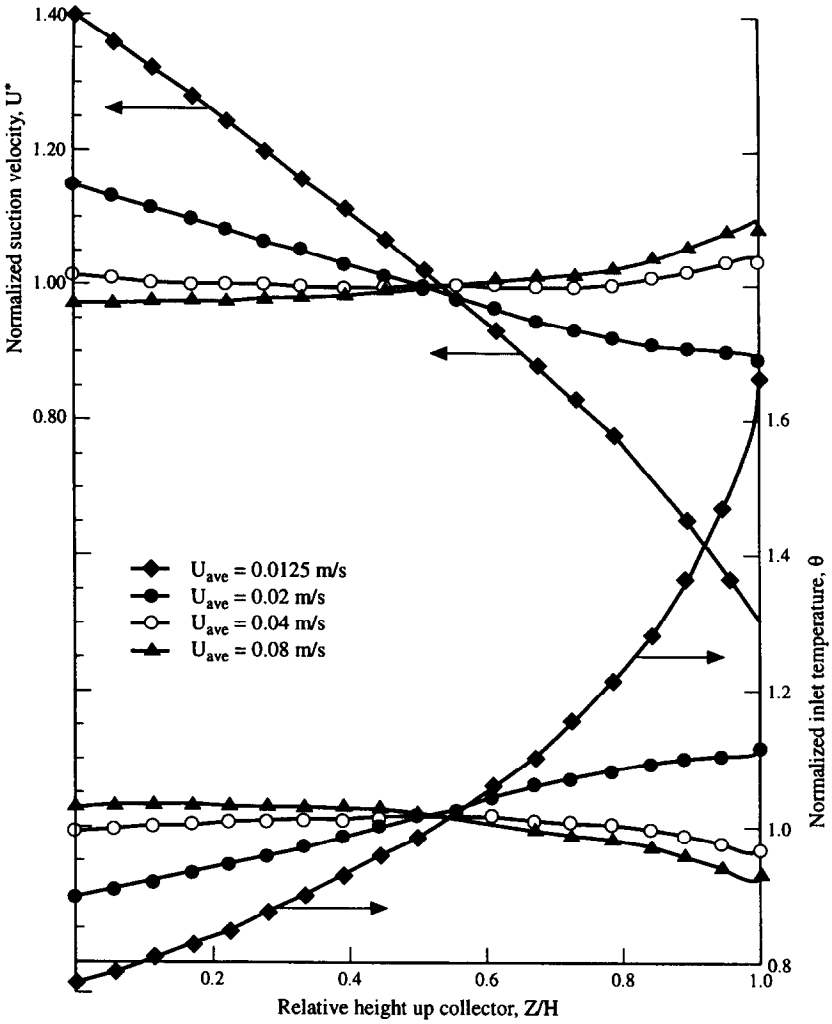

Fig. 4. Normalized suction velocity and temperature profiles for various settings of the average velocity $u_{ave,} = Q/A$. The other parametric settings are at their mid-line values.

and consider profiles of θ. The bottom part of Fig. 4 shows the θ-profile at various values of Q/A, as determined from the simulations. The shape of this profile is seen to be almost a mirror image (in the x-axis) of the velocity profile. This fact can be deduced from an energy balance on the plate and the definition of the plate effectiveness. Thus the normalized temperature profile is roughly the inverse of the velocity profile. Gunnewiek (1994) has presented a full set of graphs of θ for the situations covered in Fig (3).

(We can now examine the assumption that $U_o = h_r/\epsilon_{HX}$ is roughly constant over the height of the collector. The largest variation of U_o will occur in the case of $u_{ave} = 0.0125$ m/s in Fig. 4. In this case the suction velocity $u(t,z)$ varies by a factor of two. Examining the data of Kutscher (1992), we find that a doubling of suction velocity typically causes a 17% change in ϵ_{HX}; this means that ϵ_{HX} will vary over the collector by only $\pm 8.5\%$ from its average value. Also, elementary calculations show that the temperature variation exhibited in the bottom of the graph on Fig. 4 at $u_{ave} = 0.0125$ would cause a $\pm 8.5\%$ variation in h_r. Moreover these variations are in phase, so h_r and ϵ_{HX} both take on slightly larger values at the top of the collector and slightly smaller values at the bottom, so their ratio U_o will be even more constant. In view of this, and in view of the fact that U_o has only a modest effect in the flow distribution, it is concluded that the assumption of constant U_o should not introduce significant errors.)

The pumping pressure that the fan must develop (at least the part associated with the collector) is

$$\Delta P_{out}(H) = P_\infty - \rho g H - P_{out}(H) \qquad (7)$$

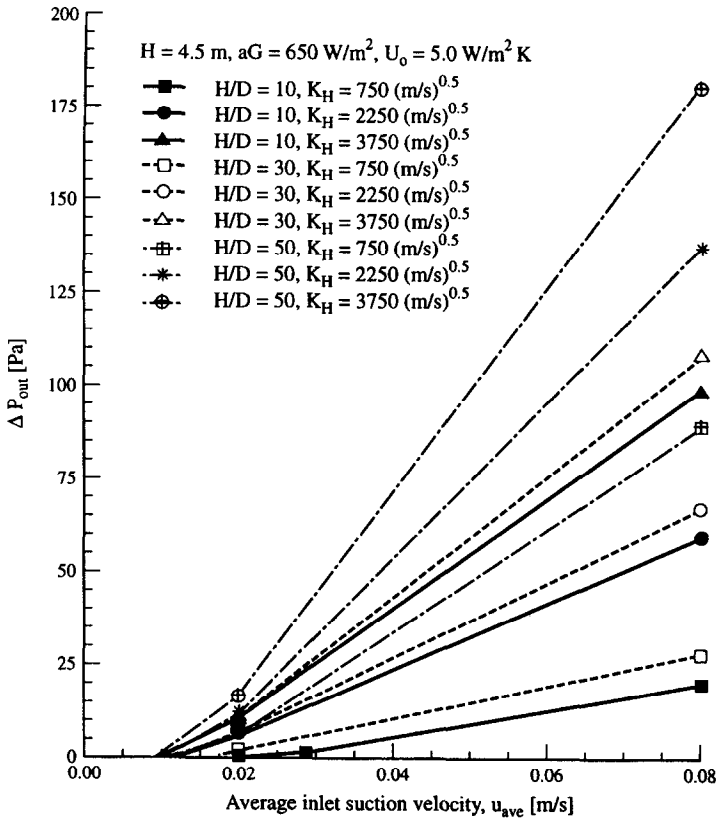

Fig. 5. Pressure difference across the plate at the top, as a function of the flow rate, for various parametric settings.

where $P_{out}(H)$ is the mass averaged pressure at the plenum exit, $z=H$. Figure 5 plots ΔP_{out} vs Q/A for various combinations of H/D and Q/A, the main two parameters tending to fix ΔP_{out}. Since ΔP_{out} is also the driving force for the suction flow at the top of the plate, negative values of ΔP_{out} indicate flow reversal—a situation that must be avoided. However, for ΔP_{out} greater than but approximately equal to zero, there is no flow reversal and, at the same time, fan work is minimized.

The relevant measure of thermal performance is the useful additional energy, q, carried by the exiting air, and this can be measured at two stations: at the plane $x=t$, where the air is just leaving the plate, and at the top exit plane $z=H$. We denote these energy rates by q_{in} and q_{out}, respectively (see Nomenclature). (The one of ultimate interest is q_{out}, but we will find it useful to consider both.) Energy rates q_{in} and q_{out} differ by the amount of heat transfer q_b taking place at the back of the plate. Thus q_b can be found from $q_b=q_{out}-q_{in}$. It can also be found by integrating $-kdT/dx$ at $x=t$ from $z=0$ to $z=H$; the fact that the two measures of q_b gave exactly the same answer acted as a check on the integrity of the CFD code, which is programmed to satisfy a global energy balance regardless of the coarseness of the grid.

Figure 6 plots q_b/q_{in} as a function of the quantity it was found to most uniquely dependent on: namely the ratio $\Delta P_{out}/\Delta P_{po}$. The numerator in this latter ratio is the quantity defined by eqn (7) and the denominator ΔP_{po} is the pressure drop across the plate when the suction is uniform: i.e. $\Delta P_o=\rho K_H(u_{ave})^{1.5}$. It is clear from Fig. 6 that q_b can represent a substantial part of the heat transferred to the air. It is also to be noted that q_b can be either positive or negative; positive q_b occurs when the plate heats the air as it rises up the plenum, and negative q_b occurs when the plate cools the air. When the flow is completely uniform (which would correspond to $\Delta P_{out}/\Delta P_{po}$ being equal to unity, since ΔP_p has to be uniform for uniform flow), q_b is zero; this is because the plenum air is all at uniform temperature, and at the same temperature as the plate. However, when $u(t,z)$ is varying, the air in the plenum at any height z will in general be different from

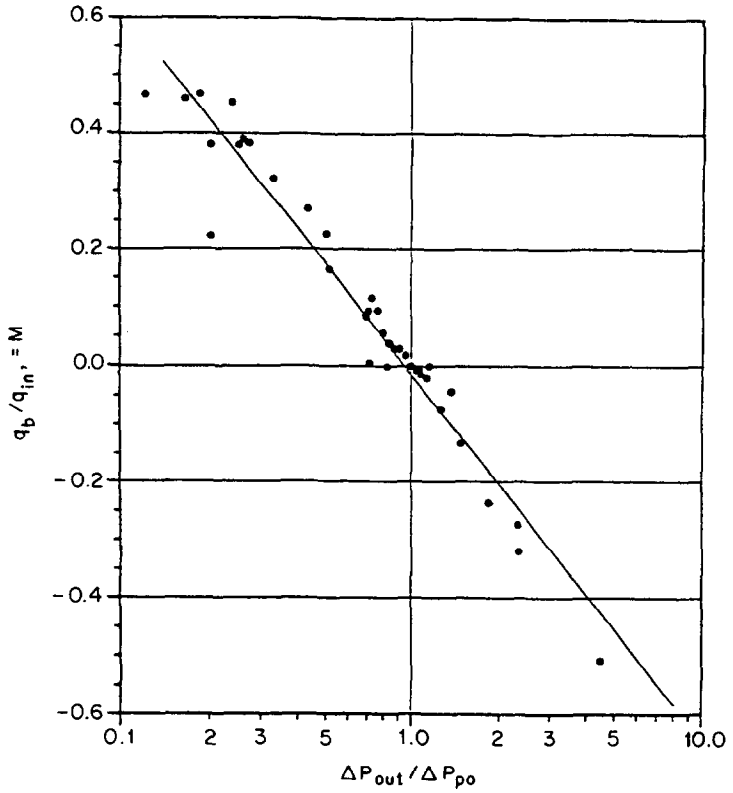

Fig. 6. A plot showing the contribution of the heat transfer at the back of the plate, as given by q_b/q_{in}, as a correlated function of the pressure difference across the plate at the top divided by the nominal pressure difference for uniform flow.

the plate temperature, and thus there is an opportunity for back heat transfer. When "forced-flow" dominates, there is greater suction at the top of the collector than at the bottom so the air enters the bottom hotter than that entering at the top. This hot air tends to be cooled by the cooler plate near the top. Thus q_b is negative when forced-flow dominates. The reverse is true when buoyant flow dominates, where q_b is positive. The pressure rate $\Delta P_{out}/\Delta P_{po}$ is an excellent measure of whether buoyant flow or forced flow is dominant (and by how much) and this explains the strong correlation shown in Fig. 6.

There are two effects of non-uniform flow on the thermal performance of a collector. The first is its effect on the heat transfer on the back of the plate, as just discussed. The second is that it may change the fraction of the net absorbed energy $(\alpha G)_n A$ that is transferred to the air as it passes through the plate. This effect is exemplified in Fig. 7, which plots η_{in}/η_{uni} where η_{in} is $q_{in}\alpha/(\alpha G)_n A$ and η_{uni}, the collector efficiency when the flow is uniform, is given by $\eta_{uni} = \alpha/(1+U_o/\rho c_p u_{ave})$. The quantity η_{in}/η_{uni} is seen to be essentially unity for all the simulations. The quantity on the horizontal axis in Fig. 7 is the coefficient of variation c_v of the suction velocity profile—the quantity that was found to most closely correlate with η_{in}/η_{uni}:

$$c_v = \int_0^1 (U^* - 1)^2 dz^* \tag{8}$$

Figure 7 shows that the non-uniform flow has only very small direct effect on the energy collected by the plate.

The main quantity of practical interest is η/η_{uni}, where η, defined by $\eta = q_{out}/(GA) = \alpha q_{out}/(\alpha GA)$, is the true collector efficiency—i.e. fraction of incident solar energy that is transferred to the fluid. The ratio η/η_{uni} characterizes how this overall efficiency differs from what it would be if the flow were uniform. The αG in the denominator of the definition for η is the actual αG, and not $(\alpha G)_n$, but one can get this αG from the equation

$$\alpha G = (\alpha G)_n \left[1 + (q_b/q_{in}) \frac{\eta_{in}}{\eta_{uni}} \cdot \frac{\eta_{uni}}{\alpha} \right] \tag{9}$$

which is readily derivable from the various definitions that have been introduced up to

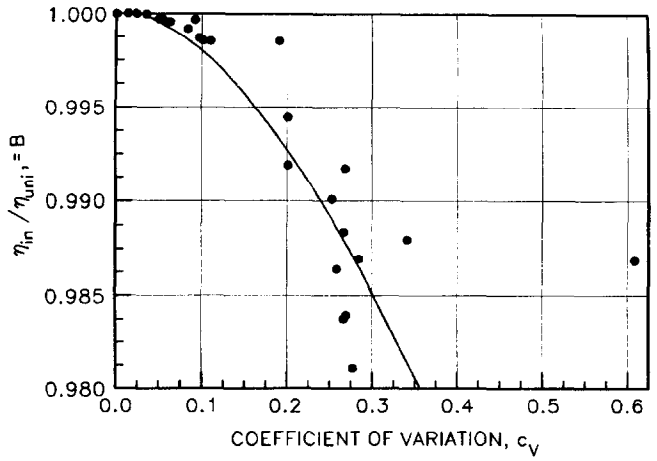

Fig. 7. A plot showing that the quantity η_{in}/η_{uni} is essentially unity over all the simulations carried out with $u_{ave} \geq 0.0125$ m/s.

now. Substituting eqn (9) for αG and $q_{in}+q_b$ for q_{out} in the definition for η, one obtains, after some re-arrangement, the desired expressions for η/η_{uni}:

$$\frac{\eta}{\eta_{uni}} = \frac{B(1+M)}{1+MB(\eta_{uni}/\alpha)}, \qquad (10)$$

where $M = q_b/q_{in}$ (from Fig. 6), $B = \eta_{in}/\eta_{uni}$ (from Fig. 7) and $\eta_{uni}/\alpha = 1/(1+U_o/(\rho c_p u_{ave}))$. As is clear from Fig. 6, B is essentially unity over the range of parameters tested. A typical value for η_{uni}/α is 0.75, so typically η/η_{uni} can range from 0.8 to 1.09 as M goes from -0.5 to $+0.5$, which is the approximate range for M in Fig. 6.

This means that non-uniform flow can actually increase the collector efficiency, but to achieve this gain in practice, one must arrange for the flow to be greater over the bottom part of the collector than over the top part; i.e. one must ensure that the flow is buoyancy-dominated. Interestingly, this is also the condition that minimizes the fan work so it has a double benefit. On the other hand, this condition is also close to the situation where reverse flow would occur (reverse flow occurs when $\Delta P_{out}/\Delta P_{po}$ in Fig. 6 goes negative).

4. CONCLUSIONS

This article has described a commercial CFD code that was specially adapted to examine unglazed transpired plate solar collectors operating under the influence of fan suction pressure and buoyancy. Special emphasis has been placed upon modelling the flow in the plenum located behind the transpired plate, to determine the importance of the six controlling parameters on the suction velocity profile. The results show a highly non-uniform profile for some of the settings of the parameters, and relatively uniform profiles for other settings. The nature of the profile depends on whether the flow is dominated by buoyancy or by the forced-flow produced by the fan. Physical reasoning is used to explain the various velocity profiles observed and the qualitative effect of each of the parameters. For Q/A less than 0.0125 m/s, reverse flow was observed, so this or smaller flows should be avoided in practice, when sizing the fan.

When the flow is non-uniform, the code predicts that an important amount of heat transfer can take place from the back of the plate to the air rising up the plenum. This heat transfer can either increase or decrease the collector efficiency, depending upon the "polarity" of the profile—i.e. depending whether the suction velocity is higher at the bottom than at the top (in which case the efficiency is predicted to be increased by the non-uniform flow), or vice versa (in which case the efficiency is predicted to decrease). The "higher-at-the-bottom" polarity is favoured in flows that are buoyancy-dominated. This means that to get the increased efficiency, the average suction velocity should be small, the plenum relatively wide, and the plate's hydraulic resistance relatively low. (See Figs 3 and 4 for a quantification of these parameter settings.) Conditions under which the efficiency can be improved by non-uniform flow are also those that keep the fan power at a minimum, so there is a dual benefit. However, the conditions are also fairly close to those corresponding to reverse flow, so the designer must take care in choosing the correct parameters.

It should be noted that this analysis has been based on certain models for the problem (e.g. uniform q_b/A, turbulent flow, constant properties, etc.) and it should be checked against experimental measurements and other, improved, formulations in the future.

Acknowledgements—Financial support of this work was provided by the Natural Science and Engineering Research Council (Canada), through a Strategic Grant. We also thank Advanced Scientific Computing Inc., 554 Parkside Dr., Waterloo, Ontario, Canada, N2L 3G1, for their assistance, and Professor Alfred Brunger for useful input.

NOMENCLATURE

A collector area, $= WH$, m^2
C_p specific heat of air at constant pressure, J/kg K
c_v coefficient of variation of suction velocity profile (eqn (8))
D plenum depth (Fig. 2), m
d distance of first node away from a wall, m
G solar irradiance on collector, W/m^2
g gravitational acceleration, m/s^2
H collector height (Fig. 2), m
h height of plenum extension (Fig. 2), m
h_r radiation heat loss coefficient from plate to ambient, $=\epsilon(\sigma T_p^4 - T_\infty^4)/(T_p - T_\infty)$, W/(m^{2}K)
K_H plate's hydraulic impedance, (m/s)$^{1/2}$
P_{ref} atmospheric pressure at ground ($z=0$), Pa
P_{out} average pressure at plenum outlet, Pa
ΔP_{out} $P_{ref} - \rho g H - \bar{P}_{out}$, Pa
ΔP_p local pressure drop across the plate, Pa
ΔP_{po} ΔP_p when flow is uniform
Q volumetric flow rate drawn out of the top of the plenum by the fan, m^3/s
q_{in} $Q\, C_p \rho(\bar{T}_{in} - T_\infty)$, W
q_{out} $Q\, C_p \rho(\bar{T}_{out} - T_\infty)$, useful heat collector collected, W
R grid expansion factor in x-direction
$T(x,z)$ air temperature at location (x,z), K
$\bar{T}_{in}$ average bulk temperature of air entering the plenum at $x=t$ face, K
$T_{i,u}$ $T(t,z)$ when $u(t,z)=u_{ave}$, K
$\bar{T}_{out}$ average bulk temperature of air at plenum exit, K
$T_p(z)$ local plate temperature, K
t thickness of plate, m
U_o h_r/ϵ_{HX}, W/m^2 K
U^* normalized suction velocity, $u(t,z)/u_{ave}$
u_{ave} $=Q/A$, m/s
$u(x,z)$ x-component of air velocity at (x,z), m/s
u_s suction velocity, m/s
$v(x,z)$ z-component of air velocity at (x,z), m/s
W width of collector (Fig. 2), m
x,y,z coordinates (Fig. 2), m
z^* z/H

Greek letters

α plate solar absorptivity
$(\alpha G)_n$ $\alpha G - q_b/A$
ϵ plate emissivity
ϵ_{HX} plate's heat exchange effectiveness (eqn (5))
η collector efficiency, $=q_{out}/(GA)$
η_{in} $q_{in}\alpha/((\alpha G)_n A)$
η_{uni} η for uniform flow, $=\alpha/(1+U_o/(\rho C_p u_{ave}))$
ρ density of air, kg/m^3
θ normalized inlet temperature (eqn (6))

REFERENCES

Bajura R. A. and Jones E. H. (1976). Flow distribution in manifolds. *J. Fluids Eng.*, **98**, 654–666.

Cao S., Hollands K. G. T. and Brundrett E. (1993). Heat exchange effectiveness of unglazed transpired-plate solar collector in 2D flow. *Proc. ISES World Congress*, 23–27 August, Budapest, Hungary, Hungarian Energy Society, Budapest, pp. 361–366.

Carpenter S. C. and Kokko J. P. (1991). Performance of solar preheated ventilation air systems. *Proc. Annual Conf. of Solar Energy Soc. of Canada*, 21–26 June, Toronto, Canada. Solar Energy Society of Canada, Inc., Ottawa, pp. 261–265.

Dymond C. S. and Kutscher C. F. (1995). A computer design model for transpired solar collector systems. *Proc. ASME/JSME/JSES Int. Solar Energy Conf.*, Maui, HA, U.S.A., March 1995. American Society of Mechanical Engineers, New York, Vol. 2, pp. 1165–1174.

Golneshan A. (1994). Forced convection heat transfer from low porosity slotted transpired plates, PhD Thesis, University of Waterloo, Waterloo, Canada.

Gunnewiek L. H. (1994). An investigation of the flow distribution through unglazed transpired-plate solar air heaters, MASc Thesis, University of Waterloo, Waterloo, Canada.

Hollick J. (1994). Personal Communication.

Kays W. M. and Crawford M. E. (1980). *Convective Heat and Mass Transfer*, 2nd Edn. McGraw-Hill, New York, pp. 178–179.

Kokko J. P. and Marshal S. (1992). Performance of the next generation of solarwalls. *Proc. of the Annual Conf. of the Solar Energy Soc. of Canada*, 4–8 July, Edmonton, Canada. Solar Energy Society of Canada, Inc., Ottawa, pp. 201–205.

Kuroda H. and Nishioka K. (1989). Heat transfer in a channel with uniform injection through a perforated wall. *J. Heat Transfer*, **111**, 182–185.

Kutscher C. F. (1992). An investigation of heat transfer for air flow through low porosity perforated plates, PhD Thesis, University of Colorado, Department of Mechanical Engineering.

Kutscher C. F. (1994). Heat exchange effectiveness and pressure drop for air flow through perforated plates with and without cross-wind. *J. Heat Transfer*, **116**, 391–399.

Kutscher C. F., Christensen C. B. and Barker G. M. (1993). Unglazed transpired solar collectors: heat loss theory. *J. Solar Energy Eng.*, **115**, 182–188.

Licharowicz A., Duggins R. K. and Markland E. (1965). Discharge coefficients for incompressible non-cavitating flow through long orifices. *J. Mech. Eng. Sci.*, **17**(2), 210–219.

Patankar S. V. (1980). *Numerical Heat Transfer and Fluid Flow*. Hemisphere, New York.